

Irudhayaraj Vinnarasi Suganya<sup>1</sup>, Sathya Seelan Kavipriya<sup>1</sup>, Anga Muthu Uma Maheswar<sup>2</sup> Gandhi Yuvasri<sup>1</sup>, Kumaresan Gayathri<sup>1</sup>, Sahaya Vincent De Paul Raj Vincent Claudia<sup>1</sup>, Sivakumar Swetha<sup>1</sup>, Thangaraj Umamathi<sup>3</sup>, Arjunan Krishnaveni<sup>3</sup> Abdulhameed Al-Hashem<sup>4</sup>, Susai Santhammal Rajendran<sup>1\*</sup>

<sup>1</sup>Corrosion Research Centre, Department of Chemistry, St. Antony's College of Arts and Sciences for Women, Dindigul. (Affiliated to Mother Teresa Women's University, Kodaikanal). Dindigul, Tamil Nadu, India, <sup>2</sup>Department of Chemistry, Sri Meenakshi Government Arts College, for Women (A), Madurai, India, <sup>3</sup>Department of Chemistry, Yadava College, Madurai, India, <sup>4</sup>Petroleum Research Centre, Kuwait Institute for Scientific Research, Kuwait

Scientific paper

ISSN 0351-9465, E-ISSN 2466-2585

<https://doi.org/10.62638/ZasMat1305>



Zastita Materijala 67 ()

(2026)

## The cannons at Dindigul Fort exemplify a remarkable accomplishment in the field of Indian Metallurgy-Exempt from corrosion

### ABSTRACT

Dindigul Fort is situated approximately 400 kilometers from Chennai in the state of Tamil Nadu, India. The fort's geographical coordinates are 10.36109°N latitude and 77.96167°E longitude. Standing at an elevation of 900 feet, the structure is predominantly constructed from granite. At this height, one can observe several brick buildings, which were likely constructed during the British colonial era. The fort is strategically located and features a circular freestanding bastion that historically housed numerous cannons. The introduction of artillery to the site can be traced back to the 17th century, and notably, these cannons have remained free from corrosion. A comprehensive examination of a rust sample collected from one of the cannons at Dindigul Fort was conducted utilizing scanning electron microscopy (SEM), dynamic light scattering (DLS), EDX and Fourier-transform infrared (FTIR) spectroscopy. This investigation identified a range of elements, such as carbon, oxygen, silicon, phosphorus, sulfur, calcium, and iron, along with the presence of nanoparticles. The FTIR spectrum served to validate the presence of  $\gamma\text{FeOOH}$ ,  $\alpha\text{FeOOH}$ , and  $\text{Fe}_3\text{O}_4$ .

**Keywords:** Cannons of Dindigul Fort, composition, SEM, FTIR, EDX, corrosion

### 1. INTRODUCTION

The monuments from earlier times serve as a valuable repository of information regarding a nation's technological advancement. India has established itself as a significant repository of archaeological and cultural heritage on the global stage. Numerous historical sites, adorned with ancient temples, monuments, and various artifacts such as pillars, sculptures, and coins, have been discovered throughout the Indian subcontinent, providing compelling evidence of the exceptional craftsmanship of ancient Indian artisans. This underscores the notion that Indian civilization was not only materially prosperous but also deeply rooted in ethical and philosophical traditions. The material development of humanity during ancient times can be understood through three major chronological phases: the Stone Age, the Bronze Age, and the Iron Age.

\*Corresponding author: Susai Santhammal Rajendran

E-mail: susairajendran@gmail.com

Paper received: 20.10.2024.

Paper accepted: 24.11.2024.

The Stone Age, the earliest segment of our prehistoric timeline, is further categorized into three distinct periods: the Paleolithic, Mesolithic, and Neolithic eras.

The preservation of historical monuments, including statues, columns, and ancient structures, requires a comprehensive analysis of the various environmental factors that lead to their degradation and affect the pace of this process. Key contributors to weathering include: (i) the deterioration of the monument's surface layer, which arises from complex microphysical processes, especially those related to moisture, with a focus on the comparative effects of rainwater and condensation; (ii) the chemical and physical interactions of pollutants in both dry and wet environments. The mechanisms of destruction are shaped by multiple elements, such as the historical significance of the monument, the nature and concentration of pollutants, and the occurrence of specific microclimatic conditions that supply the moisture necessary for chemical reactions. Therefore, it is essential to investigate the daily and seasonal variations impacting the monument, particularly in relation to heat waves and the

movement of moisture and energy. A considerable number of studies have been undertaken to explore the corrosion behavior of various prominent historical monuments [1-10]. They are presented in this section.

### **1. Chemistry of ancient materials of iron in India**

India is renowned for its extensive heritage in iron production, dating back to the protohistoric period. The ancient craftsmen demonstrated remarkable skill in creating iron artifacts with exceptional properties, reflecting their advanced knowledge in chemistry and metallurgy. Notable examples, such as the iron pillars in Delhi and Dhar, as well as the iron beams at the Sun Temple in Konark, serve as compelling evidence of this expertise. Consequently, the chemistry underlying the creation and characteristics of these ancient iron materials is a subject of great interest. Numerous researchers have examined iron artifacts from various archaeological sites across India, representing different historical periods, regions, and dynasties. A significant focus has been placed on understanding the chemistry that contributes to the remarkable features, such as the extraordinary corrosion resistance of iron pillars and cannons. This review aims to provide recent insights into iron-based materials from ancient India, with an emphasis on (1) a concise historical overview, (2) chemical composition, (3) material preparation, (4) surface microstructure, and (5) the mechanisms responsible for the unique properties of these artifacts. The analysis of these historical remains has utilized various characterization techniques, including X-ray diffraction (XRD), Proton Induced X-ray Emission, Energy Dispersive Spectroscopy (EDS), Fourier Transform Infrared Spectroscopy (FTIR), Mössbauer Spectroscopy, High-Resolution Transmission Electron Microscopy (HRTEM), and micro-particles induced X-ray emission ( $\mu$ PIXE).

The historical process of iron production utilized for the creation of high-quality wootz steel has also been examined. A comprehensive evaluation of the rust-resistant iron pillar located in Delhi has been provided. Specifically, the iron pillar at Dhar, the Adi-Mookambika temple, the iron beams at the Sun Temple in Konark, the Damascus swords crafted from wootz steel, the cannon in Thanjavur, and the iron artifacts from the Gupta period found in Eran (Madhya Pradesh) have been analyzed to gain insights into the properties of iron objects manufactured in ancient India. This research may facilitate the future creation of metallic monuments and artifacts with exceptional qualities. The findings of this review are anticipated to resonate across various fields, including but not limited to materials science, chemistry, physics, metallurgy, chemical engineering, and archaeology [1].

### **2. Use of aluminum powder for the development of a sustainable paste used in the restoration of historical monuments**

The conservation of historic sites necessitates the creation of sustainable restoration materials. This study investigated the application of aluminum powder as a primary ingredient in the formulation of eco-friendly pastes for the repair of historical monuments. These pastes currently offer a sustainable solution by incorporating aluminum powder, which possesses unique characteristics such as lightweight properties, corrosion resistance, and excellent thermal conductivity. By meticulously analyzing the mechanical, aesthetic, and sustainability dimensions of these materials, this research sheds light on the efficacy and long-term preservation benefits of pastes based on aluminum powder. The findings revealed that the developed pastes exhibit outstanding mechanical properties, including high compressive strength, excellent adhesion, and dimensional stability. Furthermore, they are visually compatible, allowing for the accurate replication of the original materials and surface textures. From a sustainability perspective, aluminum powder-based pastes contribute to waste reduction and lower the carbon footprint of restoration initiatives. The publication includes case studies that demonstrate the successful application of these pastes in the restoration of historical monuments, highlighting their effectiveness, durability, and aesthetic alignment. In conclusion, the integration of aluminum powder into environmentally friendly pastes represents a significant advancement in the preservation and restoration of historical monuments, ensuring their longevity for future generations while upholding environmental stewardship [2].

### **3. Quantifying the Potential Co-Benefit of Air Quality Improvement on Cultural Heritage in China**

Atmospheric pollutants have the potential to corrode heritage materials, particularly stone, leading to significant losses that extend beyond mere economic impacts associated with the degradation of these materials. In recent decades, traditional air pollutants have been significantly reduced in China due to clean air initiatives, yielding considerable co-benefits for the preservation of heritage. Nevertheless, these advantages may be counterbalanced by rising levels of photochemical oxidants in smog, such as ozone, which adversely affect heritage materials. This research utilized dose-response functions to evaluate the effects of air pollutants on the surface recession of limestone in heritage structures across China, while also examining the potential

advantages of improved air quality for heritage preservation. Findings indicate that the annual recession rate declined from  $9.69 \mu\text{m}\cdot\text{y}^{-1}$  in 2006 to  $6.71 \mu\text{m}\cdot\text{y}^{-1}$  in 2020, leading to a 41.4% increase in the number of heritage sites that met the ICP Materials (International Co-operative Program on Effects on Materials including Historic and Cultural Monuments) control target of  $8 \mu\text{m}\cdot\text{y}^{-1}$  for 2020. The enhancement in air quality resulted in a savings of CNY 136.2 million in maintenance costs for heritage sites. The risk of recession exhibits notable regional variations; the southern and northwest areas continue to experience higher levels of material corrosion compared to the northern and Qinghai–Tibet regions. On a national scale, PM10 (particles with an aerodynamic diameter of less than  $10 \mu\text{m}$ ) emerges as the primary risk factor contributing to the surface recession of limestone in heritage structures throughout China. This study substantiates the benefits of improved air quality for heritage conservation and offers policy recommendations aimed at enhancing heritage preservation, which include evaluating pollution risks, fostering social sustainability in heritage conservation, and implementing tailored conservation strategies [3].

#### **4. The San Carlo Colossus: An Insight into the Mild Galvanic Coupling between Wrought Iron and Copper**

The San Carlo Colossus, commonly referred to as San Carlone, is a monument featuring an internal stone pillar that supports a wrought iron framework. This framework is adorned with embossed copper sheets, which contribute to the monument's final appearance. After enduring over 300 years of exposure to the elements, this statue presents a unique opportunity to examine the long-term galvanic coupling effects between wrought iron and copper. Most of the iron components of San Carlone have been found to be in relatively good condition, with minimal signs of galvanic corrosion. However, certain iron bars exhibited a mix of well-preserved areas alongside sections displaying active corrosion. The objective of this study was to explore the potential factors associated with the mild galvanic corrosion observed in the wrought iron elements, despite their prolonged direct contact with copper. Comprehensive analyses, including optical and electronic microscopy as well as compositional assessments, were conducted on selected samples. Additionally, polarization resistance measurements were taken both *in situ* and in a controlled laboratory environment. The findings indicated that the bulk composition of the iron revealed a ferritic microstructure characterized by coarse grains. Conversely, the corrosion products on the surface were primarily identified as goethite and lepidocrocite. Electrochemical evaluations

demonstrated that both the bulk and surface of the wrought iron exhibited commendable corrosion resistance, suggesting that galvanic corrosion is unlikely due to the relatively noble corrosion potential of the iron. The limited instances of observed iron corrosion appear to be linked to environmental influences, such as the accumulation of thick deposits and hygroscopic materials that create localized microclimatic conditions on the monument's surface [4].

#### **5. Study of the catalytic action of heavy metals to understand the phenomenon of sulphation and the formation of black crusts**

The deterioration of cultural assets situated in outdoor environments is an ongoing and irreversible process, significantly exacerbated by human-induced pollution. Various degradation phenomena can manifest on stone surfaces, with the formation of black crusts being one of the most critical, particularly in areas shielded from runoff. The emergence of these degradation patinas is highly intricate, and comprehending their origins is essential for mitigating the deterioration of monuments. This research presents findings from a second exposure campaign conducted in accelerated aging chambers, aimed at elucidating the role of catalysts that initiate the sulphation process and contribute to the formation of black crusts. The study involved the analysis of Carrara marble samples treated with metal cation solutions and PM 2.5, which were subjected to three weeks of exposure in corrosion and irradiation chambers [5].

#### **6. XRF investigation of the Monument to the Fallen of the Great War by Francesco Jerace in San Ferdinando (Reggio Calabria, Italy)**

The Monument to the Fallen of the Great War in San Ferdinando (Reggio Calabria, Italy) consists of a copper-based alloy sculpture, made in the 1920s by Francesco Jerace (1853-1937), dedicated in memory of the sub-lieutenant Vito Nunziante and the fallen soldiers from the Great War. It has an important heritage value for the city of San Ferdinando, of which it is considered an identity symbol, and for Southern Italy as well. Due to its proximity and exposure to the marine environment, the monument is a key – example for the characterization of the composition of the superficial layers of the alloy and the related corrosion products, gathering important information on both the materials and the state of conservation of the sculpture. With this aim in mind, this research highlights the results of a study carried out *in situ* at elemental scale, by portable X-ray fluorescence (XRF) spectroscopy, on the occasion of the recent restoration of the monument promoted by the municipality of San Ferdinando[6].

### **7. Current state of above-ground and underground structures of the Alexander Column: an integral basis for its stability**

The Alexander Column, serving as the focal point of the architectural ensemble in Palace Square, Saint Petersburg, Russia, has consistently drawn attention from both the public and experts due to the ongoing deterioration of its granite shaft, primarily attributed to the formation of cracks. This article reviews prior research concerning the inspection and restoration of the column's shaft and other above-ground components, alongside an exploration of the factors contributing to the initiation and propagation of these cracks. An analysis of anomalies within the Fennoscandian Shield and the structural-tectonic conditions at the Montferrand quarry site has uncovered faults and circular features in the area under investigation. The study incorporates N. Hast's measurements of excess tectonic stresses in anomaly zones located in southeastern Finland, which acted horizontally and led to the emergence of tensile cracks within the granite massif, subsequently affecting the column's shaft post-installation. The most critical deformation observed in the Alexander Column is its tilt towards the northeast, a phenomenon documented in 1937 and 2000. The article further examines the construction characteristics of the column's foundations and additional subterranean elements, as well as the soil and groundwater conditions based on historical data. The contamination history of the underground environment is also considered, and an analogy-based approach is employed to evaluate the engineering-geological and hydrogeological conditions of the underground load-bearing structures in the vicinity of the Alexander Column and the New Hermitage buildings. The findings include visual assessments of the deterioration and deformation of the pavement surrounding the monument and its pedestal, which indicate the occurrence of uneven settlement of the foundation. The article concludes with overarching recommendations for establishing and executing a comprehensive monitoring system to anticipate the deformation dynamics of the Alexander Column[7].

### **8. Effect of Silicon and Nitrogen on the Microstructure and Mechanical Behavior of High-Phosphorous Steels**

Steel corrosion represents a significant economic challenge. The Delhi Iron Pillar, which possesses a high phosphorus content, has successfully resisted atmospheric corrosion for approximately 1600 years. This study focuses on the preparation of steels with 0.13 wt% phosphorus, 0.05 wt% carbon, and varying levels of silicon and nitrogen through a wrought process.

The aim is to explore the synergistic effects of silicon and nitrogen alloying additions, along with thermomechanical processing, on the mechanical properties of the steels. The influence of these alloying elements and processing techniques on the segregation of phosphorus at grain boundaries has been analyzed using Energy Dispersive Spectroscopy (EDS). The ultimate tensile strength (UTS) of the hot-forged steels exceeds 400 MPa, with elongation values surpassing 30% and  $n$  values greater than 0.3. The highest impact energy recorded is 284 J for the Fe–0.05C–0.13P–0.48Si–0.015N steel[8].

### **9. Nondestructive studies on iron pillar at Kodachadri, Karnataka, India**

We present here results of a study carried out on the iron pillar located in the Adi-Mookambika temple at Kodachadri in Karnataka, India. The iron pillar is 8.7 m high with almost square cross-section and an average perimeter of 27.5cm. The surface of the pillar is not as smooth as those at Mehrauli (Delhi) and Dhar (Madhya Pradesh). The top 1 m of the pillar shows excessive corrosion specially on the surface facing west towards the Arabian Sea, which is located about 30km away. The in situ metallography at various locations on the pillar and scanning electron microscopy on a small sample from the pillar clearly established that the iron is produced by the age-old indigenous solid-state reduction process that is used for making the so-called Adivasi (tribal) iron. Presence of slip lines in the microstructure at various locations indicates heavy forging of the iron pillar. The phosphorus content in the iron pillar is found to be much less than those reported for the iron pillars at Delhi and Dhar[9].

### **10. Influence of the Environment on the Patina of the Statue of Liberty**

The corrosion layer of copper, commonly referred to as patina, on the Statue of Liberty exhibits a range of colors that vary from one area to another, reflecting local differences in the mineral composition of the patina. It has been suggested that these color variations may result from the effects of acid rain. To explore this issue, a series of copper mineral phase diagrams has been created, illustrating the stability domains and solubilities in relation to the primary anions ( $\text{SO}_4^{2-}$ ,  $\text{Cl}^-$ ,  $\text{H}^+$ , and  $\text{HCO}_3^-$ ) present in rainwater. These diagrams serve as the foundation for a geochemical model concerning the mineralogy of the patina. The model indicates that acid rain, at the pH levels recorded in New York City's rainfall, does not influence the mineralogy or solubility of the patina. Instead, the observed color variations seem to correlate with the prevailing wind direction,

which influences the areas of the statue that come into contact with rainwater. This rainwater, in turn, favors the stabilization of sulfate copper minerals over chloride minerals. It is possible that these color patterns are now more pronounced than in previous years due to a decrease in ambient SO<sub>2</sub> levels over time[10].

The Dindigul Fort, referred to as Dindigul Malai Kottai, was built in the 16th century by the Madurai Nayakar Dynasty, alongside the Abirami Amman Kalaheswarar Temple (Figure 1). It is situated in the town of Dindigul, within the state of Tamil Nadu, India. The fort's geographical coordinates are 10.36109°N latitude and 77.96167°E longitude [11]. The fort was founded by King Muthu Krishnappa Nayakar of the Madurai Nayakar dynasty in the year 1605. In the 18th century, the fort came under the control of the Kingdom of Mysore, specifically the Mysore Wodeyars.

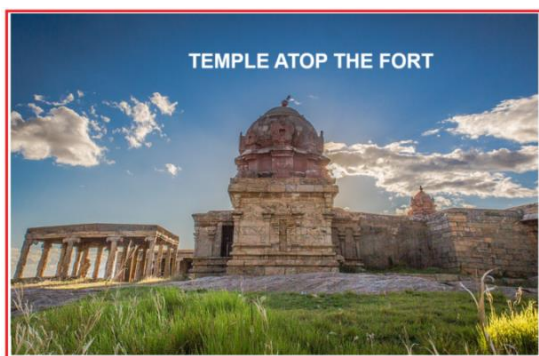


Figure 1. The Abirami Amman Kalaheswarar Temple

The fort was later seized by Hyder Ali and his son, Tipu Sultan, underscoring its strategic importance. In 1799, during the Polygar Wars, the British East India Company took control of the fort. Furthermore, an abandoned temple is located at the summit of the fort, accompanied by several heavy cannons that are still sealed with

cannonballs inside. Notably, these cannons show no signs of corrosion. This study includes an analysis of the materials used in the construction of the cannons.

## 2. EXPERIMENTAL

A small quantity of material, likely iron oxide, was removed from the cannon. This material underwent a series of analyses such as FTIR (Perkin Elmer, 1600 series), SEM, DLS and EDX (Bruker Nano GmbH Berlin, workstation, Germany).

### SEM-Analysis

SEM image of various surfaces were recorded in a CAREL ZEISS make model EVO-18

### FTIR spectra

FTIR spectra were recorded in a Perkin Elmer 1600 series model, with resolving power of 4 cm<sup>-1</sup>.

### EDX spectrum

EDX spectrum was recorded in a Bruker Nano GmbH Berlin, workstation, Germany.

### Dynamic Light Scattering technique

This technique was used to measure the size of nanoparticles distribution in a solution. For this purpose, DynaProNanoStar Dynamic Light Scattering Detector was used.

## 3. RESULTS AND DISCUSSION

### 3.1. Dindigulrockfort cannons

The rock fort rises to an elevation of 900 feet (270 meters) and has a perimeter of 2.75 kilometers (1.71 miles). During the 17th century, the fort was armed with cannons and other artillery. It was built with double walls to withstand the force of heavy weaponry. Cannons were positioned at key locations throughout the fort, along with supplies of arms and ammunition (Figure 2).

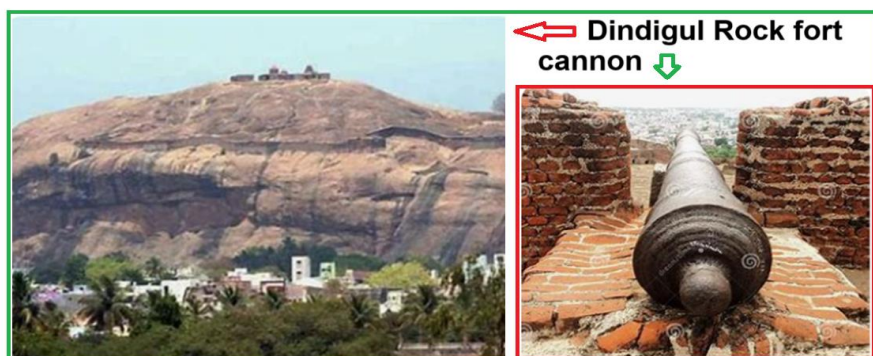


Figure 2. Cannons of Dindigulrockfort

### 3.2 Examination of the FTIR Spectrum

The FTIR Spectrum (KBr) for the iron oxide sample obtained from the cannon is presented in Figure 3.

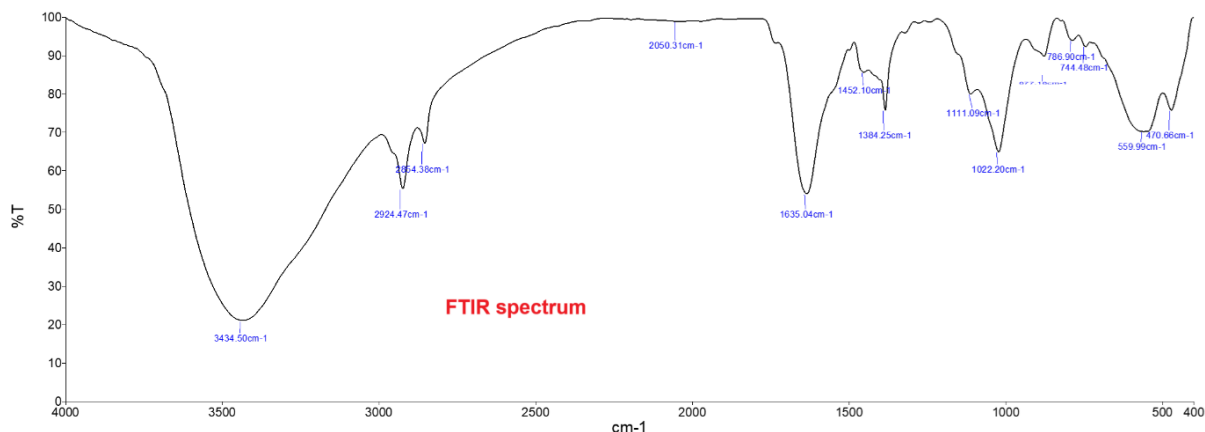


Figure 3. FTIR spectrum of the powder sample collected from the cannon

The spectral peaks clearly demonstrate the presence of  $\gamma$ -FeOOH (470.66, 1022.20, 1452.10, 1635.04  $\text{cm}^{-1}$ ),  $\alpha$ -FeOOH (786.90, 877.18  $\text{cm}^{-1}$ ), and  $\text{Fe}_3\text{O}_4$  (2924.47, 2854.38, 1635.04, 1384.25, 1022.20  $\text{cm}^{-1}$ ).

It is especially significant that magnetic iron oxide,  $\text{Fe}_3\text{O}_4$ , is recognized in the form of nanoparticles.

This layer is located in close proximity to the iron surface, succeeded by the  $\alpha$ -FeOOH layer, which is positioned at the topmost section of the cannon.

A comparable observation has been noted regarding the Delhi iron pillar. The detection of phosphorus, as demonstrated by the EDAX spectrum, further corroborates the formation of a protective iron phosphate layer on the surface of the metal.

Furthermore, iron silicate plays a significant role in enhancing the corrosion resistance of the metal. The inclusion of calcium silicate (1635.04, 2452.10, 1022.2  $\text{cm}^{-1}$ ) and calcium sulfate (1635,

1111, 1022, 560  $\text{cm}^{-1}$ ) further improves the protective properties of the metal. Iron sulfate also serves an important function in protecting the metal surface of the cannon.

### 3.3. Dynamic Light Scattering (DLS):

Dynamic Light Scattering (DLS), sometimes referred to as Photon Correlation Spectroscopy or Quasi-Elastic Light Scattering, is a technique classically used for measuring the size of particles typically in the sub-micron region, dispersed in a liquid. DynaProNanoStar Dynamic Light Scattering Detector was used.

Different facets of DLS are examined.

**Objective:** The aim is to evaluate the size distribution of small particles suspended in a solution or polymers that are dissolved within it.

**Fundamental Concept:** This technique is based on the fundamental principle of Brownian motion observed in particles, analyzing the fluctuations in the intensity of scattered light to determine the dimensions of the particles.

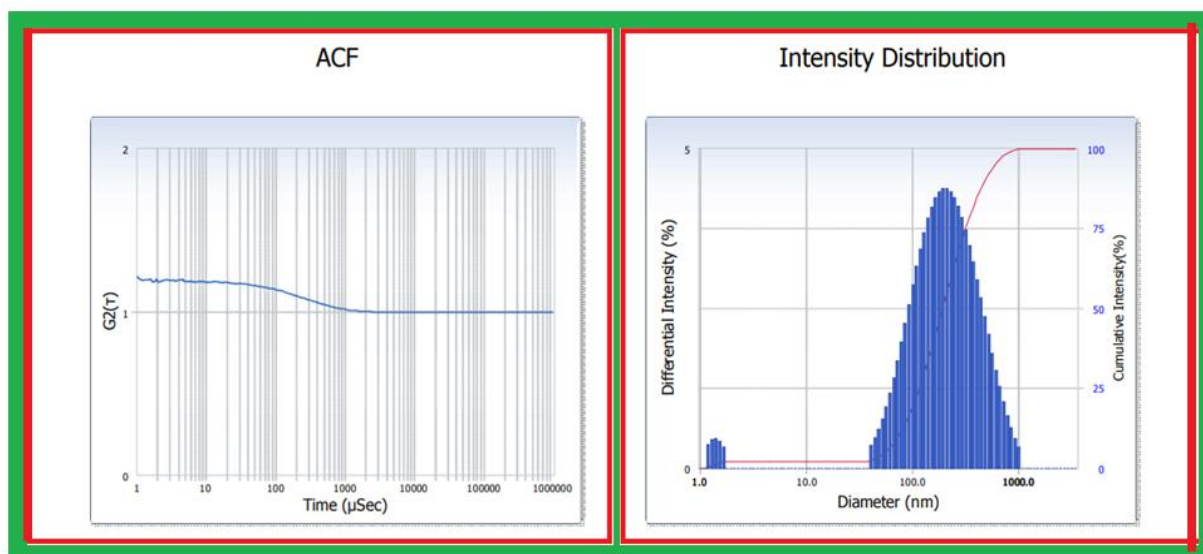


Figure 4. ACF and Intensity distribution

**Utilization:** Utilized in various fields such as pharmaceuticals, nanotechnology, and materials science for the characterization of nanoparticles, proteins, and diverse colloidal systems.

The current research examines the dimensions of the iron oxide particles along with the polydispersity index, as illustrated in Figures 4-6.

**3.4. Polydispersity index**

Polydisperse systems are characterized by a range of chain lengths, leading to an expanded molecular weight distribution. The polydispersity index (PDI) acts as a measure of the extent of this distribution. An elevated PDI indicates a broader range of molecular weights. The PDI of a polymer is calculated by the ratio of the weight average molecular weight to the number average molecular weight. Grasping the significance of the PDI is crucial for the effective selection of polymers tailored for particular applications.

**Polydispersity index = Mw / Mn**

Mw = weight average molecular weight

Mn = number average molecular weight

In the context of monodisperse polymers, characterized by uniform chain lengths (as seen in proteins), the polydispersity index (PDI) is equal to 1. The most accurately synthesized polymers, which exhibit a narrow distribution and are employed for calibration, usually present a PDI

between 1.02 and 1.10. Step-growth polymerization methods typically result in Mw/Mn ratios of approximately 2.0, whereas chain-growth polymerization can produce Mw/Mn ratios ranging from 1.5 to 20.

The polydispersity index (PI) functions as a measure of the size variability within a given sample. This variability, referred to as polydispersity, can result from the range of sizes found in the sample or from the agglomeration or aggregation of particles that may occur during isolation or analytical procedures. The PI can be quantified using instruments that utilize dynamic light scattering (DLS) or can be obtained from electron micrographs.

International standards organizations (ISOs) indicate that PI values lower than 0.05 are generally linked to monodisperse samples, while values greater than 0.7 suggest a broad spectrum of particle sizes, which is typical of polydisperse distributions (ISO standards ISO 22,412:2017 and ISO 22,412:2017).

In the current investigation, the polydispersity index (PI) is measured at 0.313. The mean particle size is determined to be 182.1 nanometers. Additionally, the diffusion constant is calculated to be  $2.702 \times 10^{-8}$ .

Distribution Results (Contin)			Cumulants Results	
Peak	Diameter (nm)	Std. Dev.	Diameter (d)	(nm)
1	1.4	0.2	Polydispersity Index (P.I.)	: 0.313
2	268.1	189.2	Diffusion Const. (D)	: 2.702e-008 (cm <sup>2</sup> /sec)
3	0.0	0.0	Measurement Condition	
4	0.0	0.0	Temperature	: 25.0 (°C)
5	0.0	0.0	Diluent Name	: WATER
Average	262.6	191.1	Refractive Index	: 1.3328
Residual	: 2.775e-003	(O.K)	Viscosity	: 0.8878 (cP)
			Scattering Intensity	: 31051 (cps)
			Attenuator 1	: 8.12 (%)

Figure 5. Cumulants results

Intensity distribution table											
Intensity Distribution Table											
d (nm)	f(%)	f(cum.%)	d (nm)	f(%)	f(cum.%)	d (nm)	f(%)	f(cum.%)	d (nm)	f(%)	f(cum.%)
7.3	0.0	2.1	58.4	1.0	5.3	464.7	2.7	87.6	3700.0	0.0	100.0
D (10%) : 76.30 (nm)			D (50%) : 200.70 (nm)			D (90%) : 505.60 (nm)					

Figure 6. Intensity distribution

**Intensity distribution table**

Intensity Distribution Table											
d (nm)	f(%)	f(cum.%)	d (nm)	f(%)	f(cum.%)	d (nm)	f(%)	f(cum.%)	d (nm)	f(%)	f(cum.%)
1.0	0.0	0.0	8.0	0.0	2.1	63.4	1.2	6.4	504.9	2.4	90.0
1.1	0.0	0.0	8.7	0.0	2.1	68.9	1.4	7.9	548.6	2.1	92.1
1.2	0.4	0.4	9.4	0.0	2.1	74.9	1.7	9.6	596.0	1.8	93.9
1.3	0.5	0.8	10.2	0.0	2.1	81.3	2.0	11.5	647.6	1.5	95.4
1.4	0.5	1.3	11.1	0.0	2.1	88.4	2.3	13.8	703.6	1.3	96.7
1.5	0.4	1.7	12.1	0.0	2.1	96.0	2.6	16.4	764.5	1.0	97.7
1.6	0.3	2.1	13.1	0.0	2.1	104.3	2.9	19.2	830.7	0.8	98.6
1.8	0.0	2.1	14.2	0.0	2.1	113.3	3.2	22.4	902.6	0.6	99.2
1.9	0.0	2.1	15.5	0.0	2.1	123.2	3.4	25.9	980.7	0.5	99.7
2.1	0.0	2.1	16.8	0.0	2.1	133.8	3.7	29.5	1065.5	0.3	100.0
2.3	0.0	2.1	18.3	0.0	2.1	145.4	3.9	33.5	1157.7	0.0	100.0
2.5	0.0	2.1	19.8	0.0	2.1	158.0	4.1	37.5	1257.9	0.0	100.0
2.7	0.0	2.1	21.6	0.0	2.1	171.6	4.2	41.8	1366.8	0.0	100.0
2.9	0.0	2.1	23.4	0.0	2.1	186.5	4.3	46.1	1485.0	0.0	100.0
3.2	0.0	2.1	25.4	0.0	2.1	202.6	4.4	50.5	1613.5	0.0	100.0
3.5	0.0	2.1	27.7	0.0	2.1	220.2	4.4	54.9	1753.2	0.0	100.0
3.8	0.0	2.1	30.0	0.0	2.1	239.2	4.3	59.2	1904.9	0.0	100.0
4.1	0.0	2.1	32.6	0.0	2.1	259.9	4.2	63.4	2069.7	0.0	100.0
4.5	0.0	2.1	35.5	0.0	2.1	282.4	4.1	67.6	2248.8	0.0	100.0
4.8	0.0	2.1	38.5	0.0	2.1	306.9	3.9	71.5	2443.4	0.0	100.0
5.3	0.0	2.1	41.9	0.4	2.4	333.4	3.7	75.2	2654.8	0.0	100.0
5.7	0.0	2.1	45.5	0.5	2.9	362.3	3.5	78.7	2884.5	0.0	100.0
6.2	0.0	2.1	49.4	0.6	3.5	393.6	3.2	81.9	3134.1	0.0	100.0
6.7	0.0	2.1	53.7	0.8	4.3	427.7	3.0	84.9	3405.3	0.0	100.0

3.5. SEM image

The scanning electron microscope (SEM) image of the powder obtained from the cannon is presented in Figure 7. It reveals the presence of extremely small particles, which are measured at the micrometer scale.

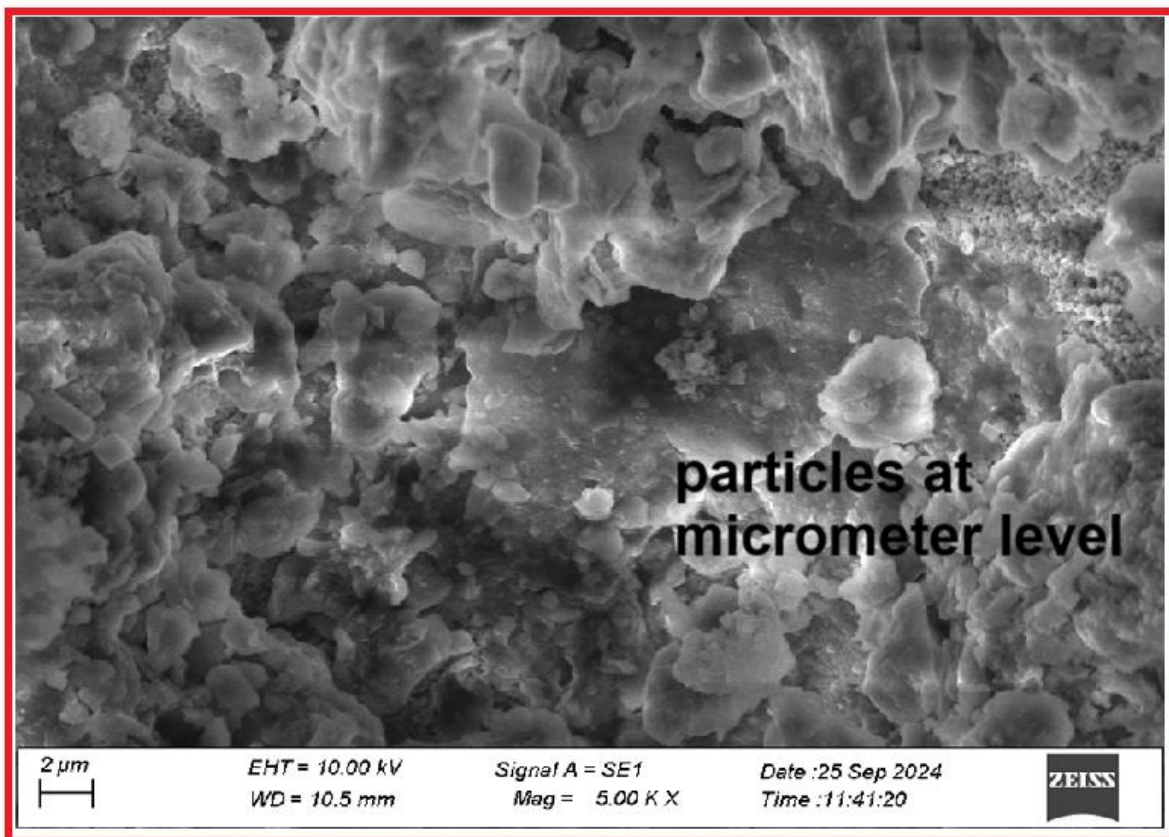


Figure 7. SEM image of Particles collected from cannon

**Energy-dispersive X-ray spectroscopy**

Energy-dispersive X-ray spectroscopy (EDS, EDX, EDXS, or XEDS), also referred to as energy dispersive X-ray analysis (EDXA or EDAX) or energy dispersive X-ray microanalysis (EDXMA), is a technique employed for the elemental analysis and chemical characterization of materials. This method is based on the interaction between a source of X-ray excitation and the sample being analyzed. Its effectiveness in characterization stems largely from the principle that each element possesses a distinct atomic structure, which results in a unique set of peaks in its electromagnetic emission spectrum. The positions of these peaks can be accurately predicted by Moseley's law, often exceeding the experimental resolution of standard EDX instruments.

To induce the emission of characteristic X-rays from a specimen, a focused beam of electrons or X-rays is directed onto the sample under investigation. In its resting state, an atom within the sample possesses ground state electrons that occupy discrete energy levels or electron shells, which are bound to the nucleus. The incoming beam can excite an electron from an inner shell,

resulting in its ejection and the formation of an electron vacancy. Subsequently, an electron from an outer, higher-energy shell transitions to fill this vacancy, and the energy difference between the two shells may be emitted as an X-ray. The quantity and energy of the emitted X-rays can be quantified using an energy-dispersive spectrometer. Since the energies of the X-rays are specific to the energy difference between the two shells and the atomic structure of the emitting element, energy-dispersive spectroscopy (EDS) facilitates the determination of the elemental composition of the specimen.

**EDX Spectrum**

EDX Spectrum was recorded in a Bruker Nano GmbH Berlin, Germany.

The EDX spectrum of the sample collected from cannon of Dindigul Rock Fort is shown in Figure 8. The elemental analysis is shown in Figure 9 .It is observed that the sample contains iron, sulphur, phosphorus, carbon, oxygen and silicon. In the present study the peaks are X-rays emitted when electrons return to the K electron shell[12].

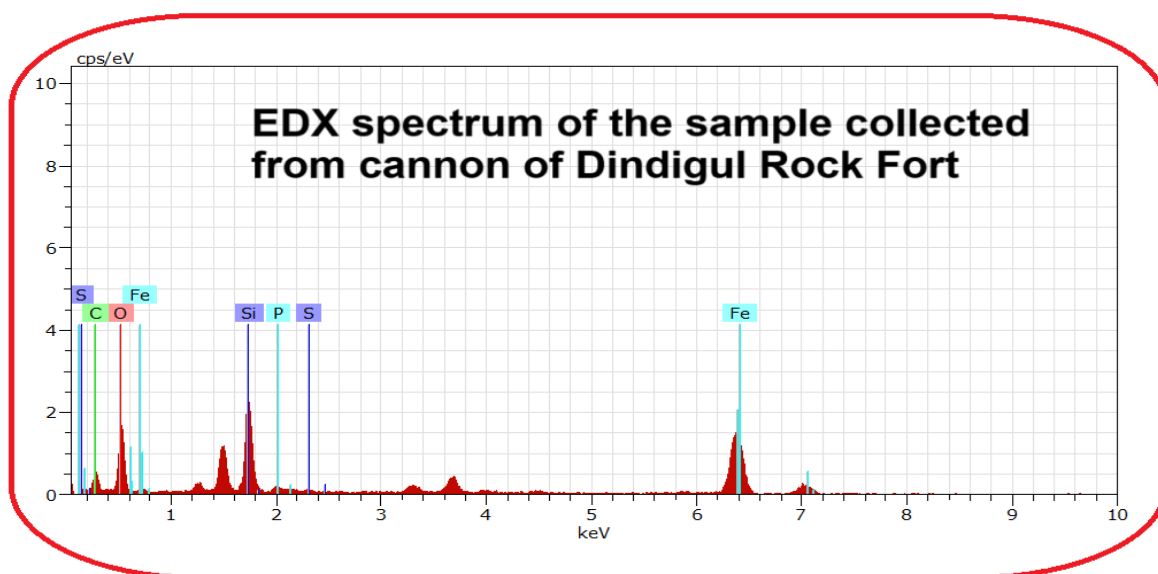


Figure 8. The EDX spectrum of the sample collected from cannon of Dindigul Rock Fort

El	AN	Series	unn. C [wt. %]	norm. C [wt. %]	Atom. C [at. %]	Error (1 Sigma) [wt. %]
O	8	K-series	35.29	46.01	49.77	5.89
C	6	K-series	20.77	27.08	39.03	4.59
Si	14	K-series	6.87	8.96	5.52	0.35
Fe	26	K-series	13.42	17.49	5.42	0.40
P	15	K-series	0.32	0.42	0.24	0.05
S	16	K-series	0.03	0.04	0.02	0.03
Total			76.70	100.00	100.00	

Figure 9. Composition of various elements

**4. CONCLUSION**

A comprehensive examination of a rust sample collected from one of the cannons at Dindigul Rock Fort was conducted utilizing scanning electron microscopy (SEM), dynamic light scattering (DLS), EDX and Fourier-transform infrared (FTIR) spectroscopy. The study leads to the following conclusions

- The FTIR spectrum indicates the existence of iron oxides.

- The measured particle size is 182.1 nm.
- The polydispersity index has been determined to be 0.313.
- It is observed from EDX study that the sample contains iron, sulphur, phosphorus, carbon, oxygen and silicon.
- The presence of  $\gamma$  FeOOH,  $\alpha$  FeOOH, and Fe<sub>3</sub>O<sub>4</sub> are confirmed.

## 5. REFERENCES

- [1] N. Agasti, B. Pani (2023) Chemistry of ancient materials of iron in India, Applied Surface Science Advances, 18, 100456, <https://doi.org/10.1016/j.apsadv.2023.100456>
- [2] M.Saba, W. Arai, G. Sabalbal, ME. Bachawati, J. Absi (2023) Use of aluminum powder for the development of a sustainable paste used in the restoration of historical monuments, E3S Web of Conferences, 436, 08001, <https://scholarhub.balamand.edu.lb/handle/uob/7091>
- [3] X.Wang, H. Li, Y. Wang, X. Zhao (2023) Quantifying the Potential Co-Benefit of Air Quality Improvement on Cultural Heritage in China, Sustainability (Switzerland), 15(11), 8709, <https://doi.org/10.3390/su15118709>
- [4] C. Petiti, C. Martini, C. Chiavari, S. Vettori, J. Marie Welter, P. Guzmán García Lascurain, S. Goidanich (2023) The San Carlo Colossus: An Insight into the Mild Galvanic Coupling between Wrought Iron and Copper, Materials, 16(5), 2072, <https://doi.org/10.3390/ma16052072>
- [5] V. Comite, A. Bergomi, P. Fermo, C. Castellano, M. Borelli, C. Andrea Lombardi, M. Formenti, C. Cavaterra, C. Della Pina (2023) Study of the catalytic action of heavy metals to understand the phenomenon of sulphation and the formation of black crusts, IMEKO TC4 International Conference on Metrology for Archaeology and Cultural Heritage, p. 1095–1100, DOI:10.21014/tc4-ARC-2023.203
- [6] F. Caridi, S. Mancini, G. Paladini, P. Faenza, V. Crupi, V. Venuti, D. Majolino (2023) XRF investigation of the Monument to the Fallen of the Great War by Francesco Jerace in San Ferdinando (Reggio Calabria, Italy), IMEKO TC4 International Conference on Metrology for Archaeology and Cultural Heritage, p.857–861, DOI:10.21014/tc4-arc-2023. 159Corpus ID: 267129695
- [7] RE.Dashko, AG. Karpenko (2023) Current state of above-ground and underground structures of the Alexander Column: an integral basis for its stability, Journal of Mining Institute, 263, pp. 757–773. Website <https://pmi.spmi.ru>
- [8] Y. Mehta, VV.Dabhade, G.P. Chaudhari (2016) Effect of Silicon and Nitrogen on the Microstructure and Mechanical Behavior of High-Phosphorous Steels Metallography, Microstructure, and Analysis, 5(5), 384–391. [https://doi.org/10.1016/S0924-0136\(02\)01131-7](https://doi.org/10.1016/S0924-0136(02)01131-7)
- [9] A. Kumar, T. Jayakumar, K. V. Rajkumar, M. M. Narayanan, G. N. Hegde, A. K. Rai, V. V. Bhat (2013) Nondestructive studies on iron pillar at Kodachadri, Karnataka, India, Current Science, 105(12), 1704–1710. <http://www.jstor.org/stable/24099752>.
- [10] R.A.Livingston (1991) Influence of the Environment on the Patina of the Statue of Liberty, Environmental Science and Technology, 25(8), 1400–1408. <https://doi.org/10.1021/es00020a006>
- [11] [https://en.wikipedia.org/wiki/Dindigul\\_Fort](https://en.wikipedia.org/wiki/Dindigul_Fort)
- [12] Energy-dispersive X-ray spectroscopy – Wikipedia

## IZVOD

### TOPOVI U TVRĐAVI DINDIGUL- PRIMER IZUZETNOG DOSTIGNUĆA U OBLASTI INDIJSKE METALURGIJE – IZUZETI OD KOROZIJE

*Tvrđava Dindigul nalazi se otprilike 400 kilometara od Čenaja u državi Tamil Nadu, Indija. Geografske koordinate tvrđave su 10,36109° severne geografske širine i 77,96167° geografske dužine. Smeštena na nadmorskoj visini od 900 stopa, struktura je pretežno izgrađena od granita. Na ovoj visini može se videti nekoliko ciglenih zgrada, koje su verovatno izgrađene tokom britanske kolonijalne ere. Tvrđava je strateški locirana i ima kružni samostojeći bastion koji je istorijski smešten u brojnim topovima. Uvođenje artiljerije na lokaciju može se pratiti do 17. veka, i primetno je da su ovi topovi ostali bez korozije. Sveobuhvatno ispitivanje uzorka rđe prikupljenog iz jednog od topova u stenovitoj tvrđavi Dindigul sprovedeno je korišćenjem skenirajuće elektronske mikroskopije (SEM), dinamičkog rasejanja svetlosti (DLS), EDX i Furijeove transformacione infracrvene (FTIR) spektroskopije. Ovo istraživanje je identifikovalo niz elemenata, kao što su ugljenik, kiseonik, silicijum, fosfor, sumpor, kalcijum i gvožđe, zajedno sa prisustvom nanočestica. FTIR spektar je poslužio za potvrdu prisustva  $\gamma$  FeOOH,  $\alpha$  FeOOH i Fe<sub>3</sub>O<sub>4</sub>.*

**Ključne reči:** Topovi tvrđave Dindigul, sastav, SEM, FTIR, EDX, korozij

Naučni rad

Rad primljen: 20.10.2024.

Rad prihvaćen: 24.11.2024.

© 2026 Authors. Published by Engineering Society for Corrosion. This article is an open access article distributed under the terms and conditions of the Creative Commons Attribution 4.0 International license (<https://creativecommons.org/licenses/by/4.0/>)